

## Electrode Material Properties and Modelling of 1-Methyl-3-octylimidazolium bis(trifluoromethylsulfonyl)imide Ionic Liquid/ Paraffin Carbon Pastes

Tesfaye T. Waryo\*, Sibusiso Qwasha, Priscilla G. Baker, Emmanuel I. Iwuoha

Department of Chemistry, University of the Western Cape, Bellville 7535, South Africa

\*E-mail: [twaryo@uwc.ac.za](mailto:twaryo@uwc.ac.za)

Received: 21 December 2015 / Accepted: 23 March 2016 / Published: 4 May 2016

A comparative study of the electrode properties of carbon pastes (CPs) composed of micro-particulate graphite powder and (1) 1-methyl-3-octylimidazolium bis(trifluoromethylsulfonyl)imide ionic liquid (IL) only (ILCP), (2) 1:1 v/v IL/ paraffin (ILPCP), and (3) paraffin only (PCP) as binder liquids was carried out with cyclic voltammetry (CV) and impedance spectroscopy (EIS). ATR-FTIR spectra and scanning electron micrographs respectively revealed that most of the graphite particles were covered with the binder molecules, and that the IL resulted in more efficient binding of particles and formation of more compact pastes than did the paraffin. In the former case the particles appeared to have been transformed into thinner sheets (flakes), i.e. fewer of graphene layers, understood as being caused by IL-enhanced exfoliation of graphene. ILCP's intrinsic capacitive current density ( $\sim 2.5 \text{ mA cm}^{-2}$ ) was 100-folds higher than that of PCP. The potential window was 2.5 V wide for ILCP and 2.2 V for ILPCP's. According to the EIS data, two conductive phases existed in ILPCP; ILCP was the least ohmic resistive paste, and that a diffusional capacitive process was involved in both. Based on the CV of  $[\text{Fe}(\text{CN})_6]^{3-/4}$  ( $E^{\circ'} \approx 0.200 \text{ V}$ ), the ILCP exhibited the highest peak currents and the highest effective electrochemical area to geometric area ratio ( $A_{\text{eff}}/A_{\text{geom}}$ ), and the PCP the lowest. However, the  $k^{\circ}$  determined by this method did not vary significantly with the paste composition. Thus, the presumed exfoliation of graphene only increased the  $A_{\text{eff}}$ . The CPs are also compared with Pt and C electrodes.

**Keywords:** Ionic liquid, 1-methyl-3-octylimidazolium bis(trifluoromethyl)sulfonyl imide, graphite, carbon paste electrode

### 1. INTRODUCTION

Room temperature ionic liquids (ILs), generally reckoned environmentally green solvents, possess good chemical and thermal stability, excellent conductivity, and show good solvation of several inorganic and organic substances [1, 2]. Of particular interest is the use of ILs as binders or

modifiers in carbon pastes (CP) as well as the electrochemical characterization of the resulting electrode materials. The attractive aspects of a CP electrode include the fact that its surface can be renewed by simple single-step polishing, and that electrochemically formed materials can be easily peel-sampled off for use in independent analysis, which is usually difficult to carry out in the case of rigid solid electrodes. Spectroscopic grade paraffin has been the most preferred binder in the preparation of such electrodes [3, 4].

The number of reports and types of ILs tested as binders or modifiers in CPs is accumulating at increasing rate [5]. These include hexafluorophosphates of 1-butyl-3-methylimidazolium (BMImPF<sub>6</sub>) [6, 7], 1-octylpyridinium (OPyPF<sub>6</sub>) [8], N-butyl-N-methyl pyrrolidinium bis(trifluoromethylsulfonyl) imide (BMPyrdNTf<sub>2</sub>) [9], 1-butyl-3-methylimidazolium (BMImPF<sub>6</sub>) [10], n-octylpyridinium (OPyPF<sub>6</sub>) [11], 4-methyl-n-octylpyridinium (MOPyPF<sub>6</sub>) [11], 4-trifluoromethyl-n-octylpyridinium (M<sub>F3</sub>OPyPF<sub>6</sub>) [11], 1-butylpyridinium (BPyPF<sub>6</sub>) [12, 13], 1-ethyl-3-methylimidazolium (EtMImPF<sub>6</sub>) [14], n-hexyl-3-methylimidazolium (HeMImPF<sub>6</sub>) [15], 1-benzyl-3-methylimidazole (BnMImPF<sub>6</sub>) [16], n-dodecylpyridinium (DoPyPF<sub>6</sub>) [17], 1-propyl-3-methylimidazolium (PMImPF<sub>6</sub>) [18], 1-hexylpyridinium (HePyPF<sub>6</sub>) [19], and 1-Butyl-1-methylpiperidinium (BMPIP<sub>PF6</sub>) [20]; tetrafluoroborates of 1-n-butyl-3-methylimidazolium (BMImBF<sub>4</sub>) [21], n-octylpyridinium (OcPyBF<sub>4</sub>) [22], 1-butyl-4-methylpyridinium (BMPyBF<sub>4</sub>) [23], 1-ethyl-3-methylimidazolium (EtMImBF<sub>4</sub>) [24], 1-Octyl-3-Methylimidazolium (OMImBF<sub>4</sub>) [25], N-butylpyridinium (BPyBF<sub>4</sub>) [25], 1-hexyl-3-methylimidazolium (HeMImBF<sub>4</sub>) [25], and 1-butyl-3-methylimidazolium (BMImBF<sub>4</sub>) [26]; bromides of 1-methyl-3-butylimidazolium (MBImBr) [27], 1,3-dipropylimidazolium (PPIImBr) [28], and 1-amyl-3-methylimidazolium (AmMImBr) [29]; bis(trifluoromethylsulfonyl)imides of 1-butyl-3-methylimidazolium (BMImNTf<sub>2</sub>) [30], (1-hexyl-3-methylimidazolium (HeMImTf<sub>2</sub>N) [31], and 1-butyl-1-methylpyrrolidinium (BMPyrdTf<sub>2</sub>N) [32]; trifluoroacetates of 1-butyl-3-methylimidazolium (BMImO<sub>2</sub>CCF<sub>3</sub>) [33] and 1-(3-chloro-2-hydroxypropyl)-3-methylimidazolium (P<sub>Cl,OH</sub>MImO<sub>2</sub>CCF<sub>3</sub>) [34]; acetates of 3-hydroxypropanaminium (P<sub>OH</sub>AmOAc) [35] and 1-(3-chloro-2-hydroxypropyl)-pyridinium (P<sub>Cl,OH</sub>PyOAc) [36]; as well as 1-ethyl-3-methylimidazolium ethylsulfate (EtMImEtOSO<sub>3</sub>) [37, 38], N-ethylimidazolium trifluoromethanesulfonate (EtImTfO) [39]; as well as chlorides of 1-(3-chloro-2-hydroxy-propyl)-3-methylimidazole (P<sub>Cl,OH</sub>Cl) [40] and 1-methyl-3-butylimidazolium (MBImCl) [41].

This paper reports new CP electrodes with (a) 1-methyl-3-octyl imidazolium bis(trifluoromethylsulfonyl)imide (MOImTf<sub>2</sub>N) as the only binder (ILCP) and (b) a 50:50 mixture of this IL and paraffin (ILPCP). These CP's electrode properties and effects on the electrode kinetics of the [Fe(CN)<sub>6</sub>]<sup>3-/4-</sup> redox system will be presented and compared with a traditional CP, i.e., paraffin as the only binder (PCP), glassy carbon (GC) and platinum (Pt) electrodes.

## 2. EXPERIMENTAL

### 2.1 Chemicals

1-Methyl-3-octylimidazolium bis(trifluoromethylsulfonyl)imide (MOImTf<sub>2</sub>N) and graphite powder (natural micro crystals, Aps 2-15 microns, 99.9995 %) were respectively obtained from Merck

(South Africa) and Alfa Aesar (USA). Paraffin oil (Spectranal) was obtained from Riedel-De Haen.  $K_3Fe(CN)_6$  (98%) was obtained from Sigma Aldrich. MOImTf<sub>2</sub>N (*density* = 1.33 g/ mL), a hydrophobic IL with conductivity of about 1.6 mS cm<sup>-1</sup> [42], is twice as viscous (90.80 mm<sup>2</sup>/ s) as paraffin (*d* ~ 0.827-0.890 g/ mL). Solutions were prepared using ultrapure de-ionized (DI) water (18 MΩ cm) from a RiOs™ 3/ Synergy/Millipore system.

## 2.2 Preparation of the Carbon Paste (CP) Electrodes

The PCP was prepared by thoroughly mixing 0.30 g of the graphite powder and 200 μL of paraffin oil using an agate mortar and pestle for 20 min until a visually uniform consistency [2, 6, 43]. The ILCP was prepared same way but using the IL. In case of the ILPCP, 100 μL of paraffin and 100 μL of MOImTf<sub>2</sub>N were simultaneously added. The resulting CPs were then transferred into separate glass vials, compacted and let to stand overnight. To prepare electrodes, small portion of a paste was taken out with polyethylene splinter and packed 3 mm deep in a Teflon tube with internal copper wire electrical contact. The CP working electrodes made this way were always gently polished over a white photocopy paper in order to generate fresh surfaces and rinsed with water prior to each experiment.

## 2.3 Instrumentation

Cyclic voltammetry and impedance spectroscopy measurements were carried out using a three electrode cell (CP working, a Pt wire auxiliary, and an Ag/AgCl (3 M NaCl) reference electrodes), the PAR 273A potentiostat connected to a Lock-in amplifier (Signal Recovery, Model 5210), and the PowerSuite software (Ver. 2.46, AMETEK, INC., PA, USA). The supporting electrolyte (aq. KCl, 0.1 M) was always purged with ultrapure Ar gas (Afrox, South Africa) and kept under Ar-blanket during measurements. Complex non-linear least square (CNLS) of impedance data to equivalent circuit models was carried out using Z-View software (Ver 3.1c, Scribner Assoc., Inc., NC, USA), at Chi-squared and Sum of Squares of about 10<sup>-3</sup> and 0.1 or less, respectively, and component errors of <5%. SEM images were obtained with JEOL- JSM 7500F field emission electron microscope, and the ATR-FTIR absorption spectra with Model spectrum 100 STIR spectrometer (PerkinElmer). Potential windows of the electrodes in aq. KCl were first established by recording cyclic voltammograms (CVs) of the CP electrodes at 0.1 V/ s.  $[Fe(CN)_6]^{3-}$  was used as a redox probe. Prior to use, the Pt and GC disc electrodes were first successively polished with 1, 0.5, and 0.03 μm Al<sub>2</sub>O<sub>3</sub> powder aq. slurries, and then sonicated in water bath and rinsed with water.

# 3. RESULTS AND DISCUSSION

## 3.1 FTIR Absorption and Microscopic Characteristics

In Figure 1, the ATR-FTIR spectra and SEM images (inset) of samples the PCP (a), ILPCP (b), ILCP (c), and pristine graphite powder (d) are shown. In (d), isolated and irregularly oriented multi-

layered graphite particles were observed, obviously since the powder was not processed into a paste. In contrast, well-compacted and relatively more aligned flakes were observed for each paste due to the presence of a binding liquid and the process of preparation. When comparing the images with each other, one can see that MOImTf<sub>2</sub>N, hence forward simply referred to as “the IL”, enhanced the inter-particle binding and yielded more compact pastes relative to the paraffin oil.

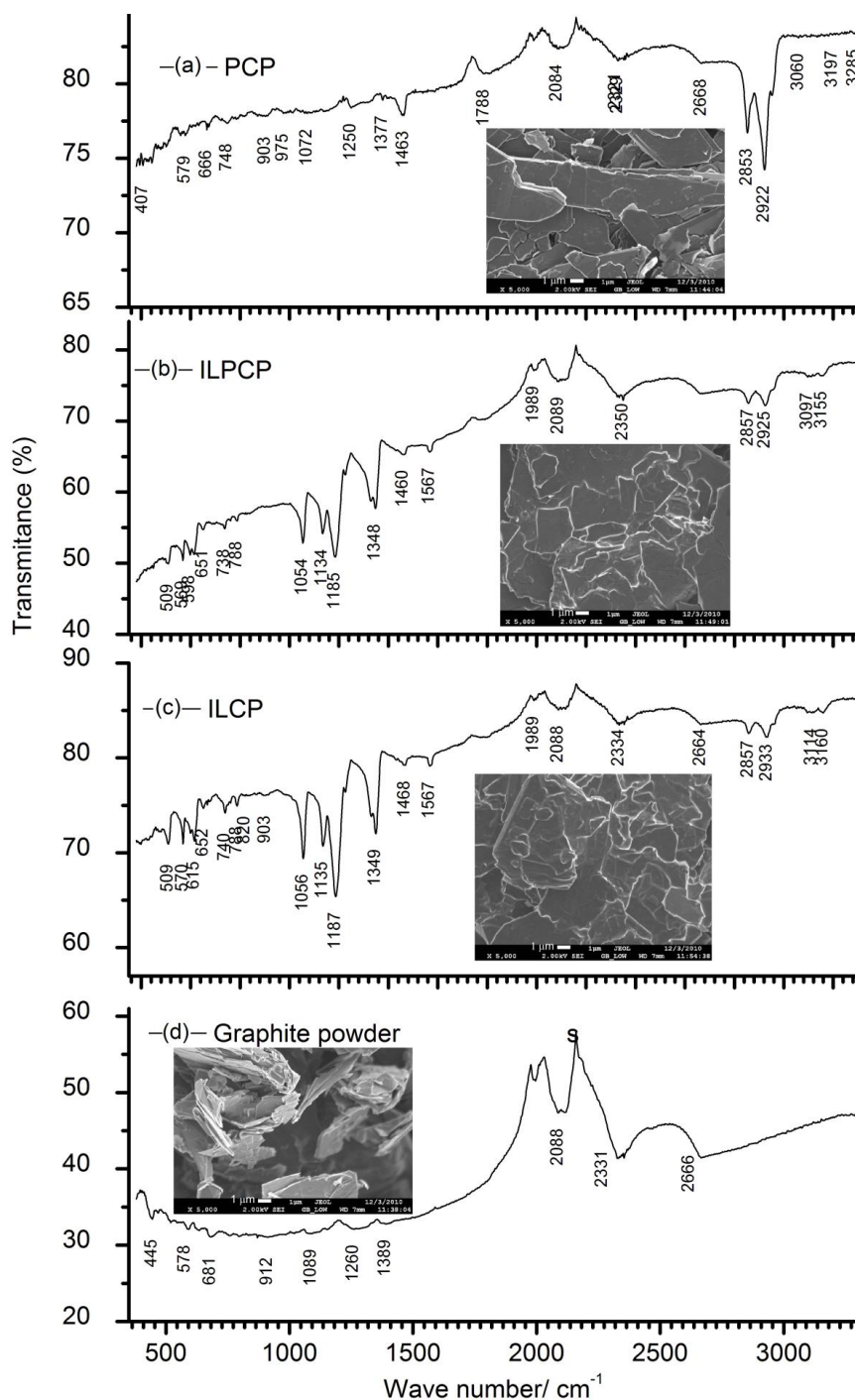


**Figure 1.** ATR-FTIR spectra and SEM images (inset) of PCP (a), ILPCP (b), ILCP (c), and pristine graphite powder (d) samples

This may be ascribed to the IL's higher viscosity and ions which can make stronger electrostatic interactions with surface functional groups of the graphite particles, effectively ionising the latter so that arrays of sandwiched counter ions hold the particles together. SEM image data in previous reports show that other ionic liquids like  $\text{BM}^+\text{BF}_4^-$  [26],  $\text{OPyPF}_6$  [44] and  $\text{BPyr}^+\text{PF}_6^-$  [45] also impart similar effects on the consistency of a CP. It has also been proposed that the IL might encourage exfoliation of graphene layers during paste preparation in order to account for the observed single-sheet flakes instead of the multi-layered graphite particles in ILCPs [44, 46].

The assignment of the above peaks was done with the help of textbook [47, 48] and handbook [49] IR-absorption peak tables and correlation charts. The pristine graphite powder (Figure 1(d)) exhibited the absorption peak features at  $2088\text{ cm}^{-1}$ ,  $2331\text{ cm}^{-1}$ , and  $2666\text{ cm}^{-1}$ . These peaks, as hallmarks of surface residing graphite particles in the pastes, were indeed observed for all pastes. However, the first distinct effect of the paste formation process, regardless of the binder type, was the drastic shift of the base-lines to higher transmittance: from about 40% to over 80%. Thus, surfaces of most graphite particles were subsequently covered with molecules of the binder liquids. It is known that paraffin is a mixture of a wide range of medium-chain length, liquid alkanes with very low volatility. The peaks attributed to its molecules in the spectrum of the PCP (Figure 1(a)) were  $2922\text{ cm}^{-1}$  ( $\nu_{\text{as}}\text{CH}_2$ ),  $2853\text{ cm}^{-1}$  ( $\nu_{\text{as}}\text{CH}_3$ ),  $1463\text{ cm}^{-1}$  ( $\delta_{\text{as}}\text{CH}_3$ ),  $1377\text{ cm}^{-1}$  ( $\delta_{\text{s}}\text{CH}_3$ ),  $748\text{ cm}^{-1}$  ( $\delta\text{CH}_3$  rocking).

Based on the higher number of functional groups in IL molecules than in paraffin ones, the former imparted for far more number of absorption peaks than the latter (Figure 1(c)). Because of its alkyl groups (1-methyl or 3-octyl), the IL also exhibited some paraffin-like peaks at  $2933\text{ cm}^{-1}$  ( $\nu_{\text{as}}\text{CH}_2$ ),  $2857\text{ cm}^{-1}$  ( $\nu_{\text{as}}\text{CH}_3$ ), and  $1468\text{ cm}^{-1}$  ( $\delta_{\text{as}}\text{CH}_3$ ). However, these common peaks were relatively weaker and blue-shifted (by about  $5 - 10\text{ cm}^{-1}$ ) relative to the corresponding peaks of paraffin. This was probably because, these functional groups are in a lower concentration and belong to alkyl groups bonded to the N atom in the IL unlike their free counterparts in paraffin. The rest of the peaks were assigned as follows:  $\nu_{\text{s}}(\text{C-F})$  at  $1135$  or  $1187\text{ cm}^{-1}$ ,  $\nu(\text{CF}_3) = 1349\text{ cm}^{-1}$ ,  $652\text{ cm}^{-1}$ ,  $615\text{ cm}^{-1}$ ,  $570\text{ cm}^{-1}$ , and  $509\text{ cm}^{-1}$ ;  $\nu_{\text{as}}(\text{R}_2\text{SO}_2) = 1349\text{ cm}^{-1}$ ;  $\nu_{\text{s}}(\text{R}_2\text{SO}_2) = 1187\text{ cm}^{-1}$ ; and  $\nu(-\text{C}=\text{N}^+-\text{R}_2) = 1567\text{ cm}^{-1}$ . The absence of the  $\nu_{\text{s}}(\text{N-H})$  peak near  $3500\text{ cm}^{-1}$  (range not shown) is also a hall mark of the IL.

### 3.2 Voltammetric and Impedimetric Characteristics of CP/Aq. KCl Interfaces

#### 3.2.1 Potential –windows and other electrode features

Figure 2 displays CVs of ILPCP, ILCP, PCP, GC, and Pt electrodes in aq. KCl (0.1 M). The respective limits of polarization (potential windows) were from  $+1.5$  to  $-1.8\text{ V}$  (ILCP),  $+1.5$  to  $-1.8\text{ V}$  (ILPCP),  $+1.5$  to  $-1.7\text{ V}$  (PCP),  $+1.5$  to  $1.5\text{ V}$  (GC), and  $+1.2$  to  $-1.0\text{ V}$  (Pt). The IL resulted in carbon pastes with higher double-layer charging current density ( $I_{\text{dl}}$ ) or noise relative to paraffin. For instance, the  $I_{\text{dl}}$  for ILPCP was about 100-fold of the  $I_{\text{dl}}$  for PCP (ca.  $5\text{ }\mu\text{A cm}^{-2}$  at  $0.1\text{ V/s}$ ). The former's residual Faradaic peaks were also much higher (about 50-folds) than that of the latter (ca.  $70\text{ }\mu\text{A cm}^{-2}$  at  $0.1\text{ V/s}$ ). If purely double-layer charging current regions only were to be considered, the corresponding windows would be from  $+1.4$  and  $-1.6\text{ V}$  for PCP and from  $1.00$  to  $-1.00\text{ V}$  for ILPCP. ILCP's background current was even much higher, being about 10-fold of that of the ILPCP. Overall, this

property varied as follows:  $I_{dl}(\text{ILCP}) > I_{dl}(\text{ILPCP}) > I_{dl}(\text{Pt}) > I_{dl}(\text{GC}) > I_{dl}(\text{PCP})$ . The observed increase in  $I_{dl}$  because of the IL is in accordance with previous studies on IL-modified CP electrodes [6, 50]. Possible causes include faradaic processes related with electroactive impurities in the IL, ionic-migration within the CP, ion-enhanced double-layer charging phenomena, as well as ion-transfer phenomena across aqueous-IL interfaces [51].

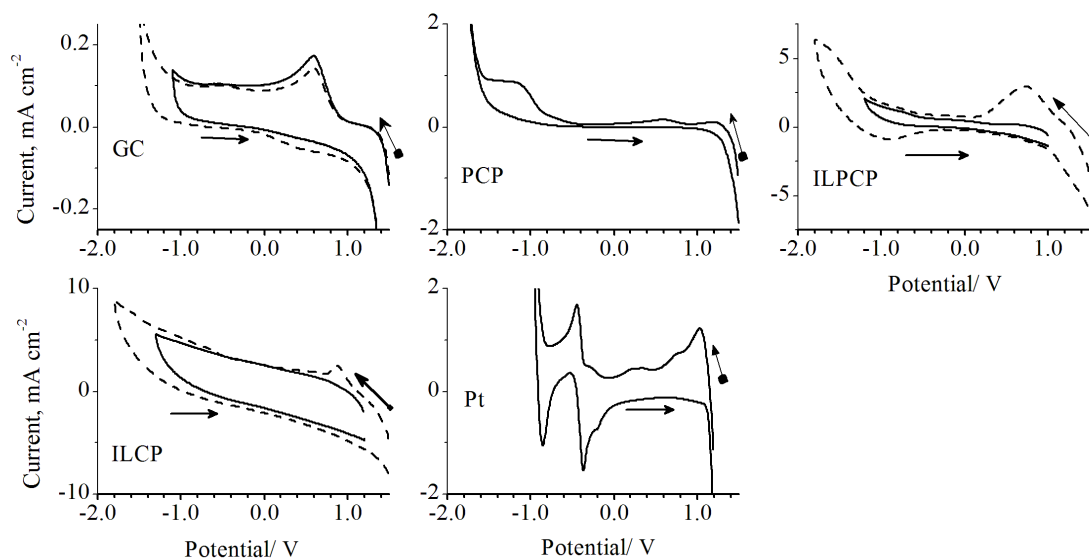


**Figure 2.** Potential windows and area-normalized CVs of various electrodes in aq. KCl (0.1 M). Scan rate: 100 mV/ s.

On the other hand, ILPCP and ILCP potential windows were indeed wide enough and, thus, these CP materials can provide electrochemically inert surfaces for electrochemical studies of electroactive substances.

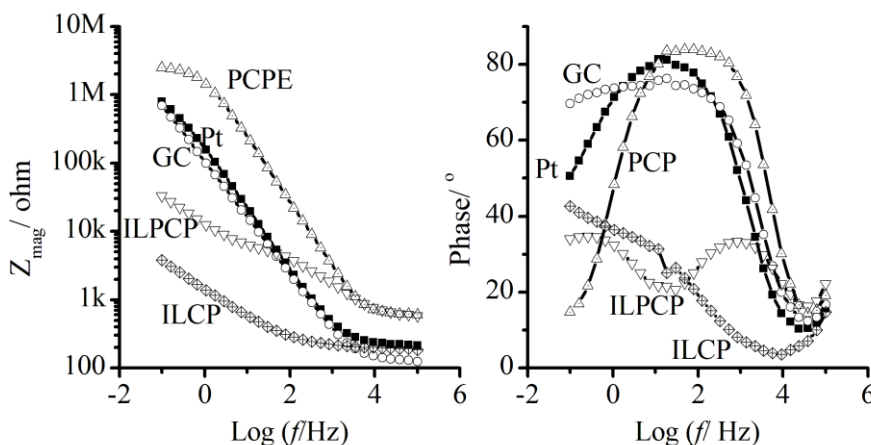


**Figure 3.** Bode plots for the CP, Pt, and GC electrodes in aq. KCl (0.1 M).  $E_{ac} = 10$  mV,  $f = 0.1$  to  $10^5$  Hz, bias  $E_{dc} = 0.200$  V except for ILCP for which  $E_{dc} = 0.170$  V.

However, a slight leaking of the IL from the ILCP electrode into the supporting electrolyte was observed at potentials beyond 1.2 V or -1.3 V. Thus, in subsequent experiments the potential scan range for this electrode was set from 1.2 V to -1.3 V, which was still wider than the working ranges of the ILPCP (1.0 V to -1.2 V) and Pt electrodes (1.2 V to -0.9 V) as set in order to exclude the corresponding residual background peaks. Hence, from practical considerations, the PCP exhibited the widest working potential range (1.5 V to -1.7 V) and the GC exhibited the second widest one (1.5 V to -1.5 V). Nevertheless, the ILCP in particular, and, somehow, the ILPCP as well, offered much smoother background CVs than Pt and GC (Figure 2). Furthermore, the high intrinsic current density characteristics make ILCP and ILPCP promising candidates for applications in super-capacitors [52].

### 3.2.2 Electrochemical impedance modelling

Figure 3 shows overlaid impedance spectra (Bode plots) of the three CPs, GC, and Pt electrodes in aq. KCl (0.1 M). The PCP exhibited more or less a single time-constant spectrum like Pt and GC, thus it could be modelled with simple Randles cell (Figure 4 (a)) composed of an uncompensated resistance ( $R_{u-t}$ ) in series with a parallel circuit ( $CPE1//R_{ct1}$ ) of a constant phase element (CPE1) and a charge-transfer resistor ( $R_{ct1}$ ) as in previous literatures on PCP electrodes in the presence of electroactive moieties [45, 53 - 55] – but less the Warburg diffusion element. Since these impedance spectra were obtained in a blank electrolyte,  $R_{ct1}$  could be taken as lump-sum manifestation of background electron transfer processes involving trace electroactive impurities.

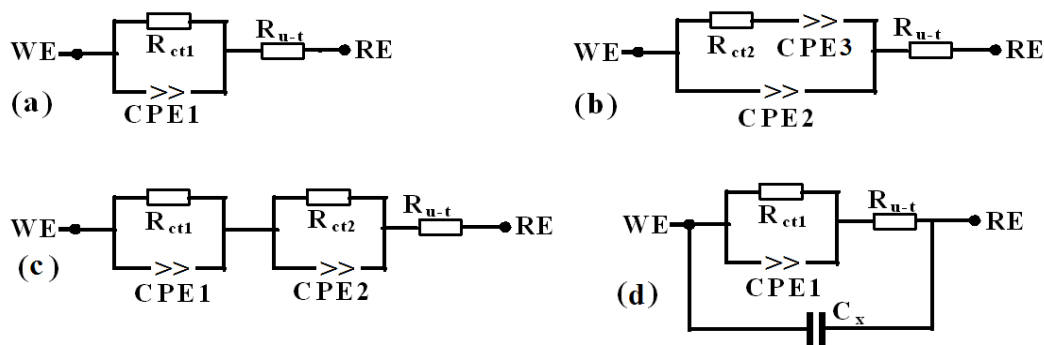


**Figure 4.** Equivalent circuit models for the electrode/ electrolyte interfaces in aq. KCl (0.1 M) for (a) PCP, Pt and GC, (b) ILCP, and (c) ILPCP electrodes. The high frequency capacitive arcs were accounted for by including a capacitor ( $C_x$ ) as in (d).

The model that fit ILCP's impedance spectrum is shown in Figure 4(b), after a slight modification of Figure 4(a) in which CPE1 is replaced by CPE2, and  $R_{ct1}$  by  $R_{ct2}$  connected in series with CPE3. Unlike  $R_{ct1}$ , probably  $R_{ct2}$  represents an ionic charge-transfer resistance because such a process is now possible from the IL layer or channels to the aq. phase and back [5]. The CPE3 element would then represent an infinite diffusion Warburg impedance ( $Z_{W,\infty}$ ) related this ion transfer process. In contrast, the ILPCP/ aq. KCl interface exhibited a two time-constant spectrum, possibly because this paste was microscopically segregated into two distinct phases. This is consistent with models

suggested in previous reports for traditional CPs modified with other ILs [6]. Thus it may be modelled by the equivalent circuit in Figure 4 (c) in which model (a) and (b) have been combined less the CPE3 component. Thus, the two phases of ILPCP at the electrode/aq. KCl interface were not identical to either of the pristine CP and ILCP phases. Furthermore, in each impedance spectrum, the rise in phase angle in the high-frequency extreme region was understood according to literature [56] to be a capacitive artefact, and indeed, appending an external parallel capacitor ( $C_x$ ) to each electrical model as shown in Figure (d) resulted in a better fitting of the entire spectra. The fitted values of  $C_x$  were consistently about 1 - 2 nF, thus it possibly originated from the same noise source regardless of the electrode.

CNLS fitting of the EIS data in Figure 3 to the respective models in Figure 4 yielded the values in Table 1 for  $R_{u-t}$  and  $R_{ct}$  as well as the  $Z_{CPE}$  (CPE impedance) parameters  $T_{CPE}$  and  $P_{CPE}$  in Equation-1[57-59], whereas the exchange current densities ( $I_o$ ) were estimated according to Equation-2 [60];  $\omega$  being the angular frequency of the ac excitation potential waveform in  $\text{rad s}^{-1}$ ,  $n$  is number of electrons per reaction,  $R = 8.31 \text{ J K}^{-1} \text{ mol}^{-1}$ ,  $T$  is temperature in K,  $F = 96485 \text{ C mol}^{-1}$ , and  $A$  is electrode area in  $\text{cm}^2$ .  $T_{CPE}$  is a scale coefficient while  $+1 \geq P_{CPE} \geq -1$ . When  $P_{CPE}$  equals +1, 0, or -1, a CPE could be re-interpreted respectively as a pure capacitor, or resistor, or inductively behaving processes, and then the  $T_{CPE}$  as the corresponding capacitance ( $C$ ), or inverse resistance ( $1/R$ ), or inverse inductance ( $1/L$ ) parameter. In a limited frequency segment, a CPE with a positive fractional value of  $P_{CPE}$  is usually understood as a distributed RC circuit; and when negative, as a distributed RL circuit. For  $P_{CPE}$  of 0.5, the CPE could be re-interpreted as an infinite-diffusion Warburg impedance ( $Z_{W,\infty}$ ), if applicable, and in which case  $T_{CPE}$  would be equated with the inverse of the Warburg coefficient ( $1/\sigma_{W,\infty}$ ).

$$Z_{CPE} = \frac{1}{T_{CPE} \times (i\omega)^{P_{CPE}}} \quad \text{(Equation-1)}$$

$$I_o = \frac{RT}{nFAR_{ct}} \quad \text{(Equation-2)}$$

**Table 1.** Equivalent circuit characteristics and physical quantities extracted after CNLS fitting of the EIS results in Figure 3 for various electrodes in 0.1 M KCl. \*These values are for CPE3

	$A_{geom}/\text{cm}^2$	$R_{u-t}/\Omega$	$R_{ct}/\text{k}\Omega$	$T_{CPE}/10^{-6} \text{ s}^p \Omega^{-1}$	$P_{CPE}$	$\sigma_{W,\infty}/10^3 \Omega \text{ s}^{-P}$	$P_{W,\infty}$	$\rho_{ele}/\Omega \text{ cm}$	$A_{geom}R_{ct}/\text{k}\Omega \text{ cm}^2$	$T_{CPE}/A_{geom}/10^{-6} \text{ s}^p \Omega^{-1} \text{ cm}^{-2}$	$I_o/\mu\text{A cm}^{-2}$
Pt	0.0201	225	1366	1.18	0.88			0.00	28	58.7	0.933
GC	0.0707	128	6800	1.97	0.84			0.00	480	27.9	0.0534
PCP	0.0201	610	2420	0.0825	0.95			28	49	4.1	0.528
ILPCP	0.0201	494	4.6	2.8	0.63			20	0.049	280	524
			96	35.2	0.58				0.96	3520	26.7
ILCP	0.0314	191	3.5	221	0.55	5.68*	0.59*	0.00	0.110	7038	233

As  $R_{u-t}$  is simply the sum of un-compensated resistances of the electrolyte solution ( $R_{u-s}$ ) and the electrode material ( $R_{u-m}$ ), the differences in  $R_{u-t}$  between two electrodes was taken as being due to the resistance difference between the materials. According to literature, the typical resistivity ( $\rho$ ) of Pt ( $1.1 \times 10^{-5} \Omega \text{ cm}$ ) is less than 1% of that of a GC ( $3.02 \times 10^{-3} \Omega \text{ cm}$ ) and a graphite ( $0.5 - 3.5 \times 10^{-3} \Omega \text{ cm}$ ) materials [61-65]. The Pt and GC electrodes used in this study were made of imbedded Pt and GC discs with thicknesses of about 0.40 cm and 0.330 cm, and cross-sectional areas of  $0.0201 \text{ cm}^2$  and  $0.0707 \text{ cm}^2$ , respectively. This means, the  $R_{u-m}$  for these two electrodes could be about  $2.19 \times 10^{-4} \Omega$  (Pt) and  $1.41 \times 10^{-2} \Omega$  (GC), and, thus, so small that the  $R_{u-t}$  measured in these cases should be effectively the same as the  $R_{u-s}$  of the electrolyte. Thus the  $R_{u-s}$  ranged from about  $\sim 128$  to  $225 \Omega$  (see Table 1), varying from experiment to experiment due to the inconsistency in the working electrode - reference electrode positioning. As the  $R_{u-t}$  in case of ILCP was not different, the resistance of this material was also insignificant compared to that of the electrolyte. Conservatively setting the latter at  $200 \Omega$ , the resistivity ( $\rho_{ele}$ ) of PCP and ILPCP were then respectively estimated to be  $28 \Omega \text{ cm}$  and  $20 \Omega \text{ cm}$ . Thus, the ILCP not only exhibited the smallest ohmic resistivity among the CPs, but it was also much less resistive than the electrolyte as were the GC and Pt electrodes.

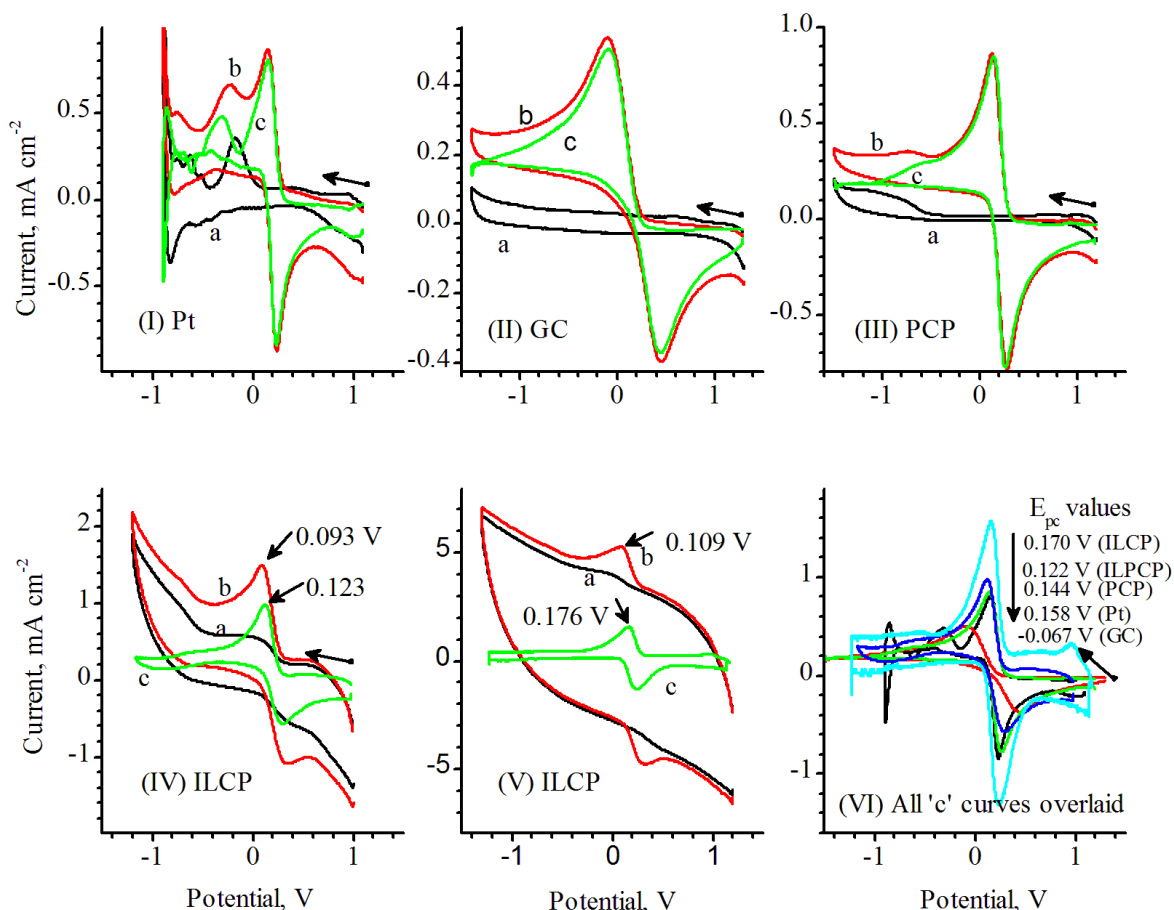


**Figure 5.** Area-normalized CVs of  $[\text{Fe}(\text{CN})_6]^{3-}$  (4 mM) recorded at 100 mV/s in aq. KCl (0.1 M) without (curves 'c') and with (curves 'b')  $iR$ -drop and  $I_{bg}$  corrections. Curves 'a' are uncorrected background CVs at 0 mM.

Based on the values of the  $P_{CPE}$  parameter, the PCP electrode ( $P_{CPE} = 0.95$ ) was slightly smoother and more polarizable than the two solid electrodes, Pt ( $P_{CPE} = 0.88$ ) and GC ( $P_{CPE} = 0.84$ ). The ILCP exhibited a  $P_{CPE}$  of about 0.55, thus its surface was either highly contorted or complicated by ionic multi-layer capacitors as well as incessant ionic migration and leakage processes. The ILPCP was characterized with two values of  $P_{CPE}$ , 0.63 and 0.58 corresponding the two phases as described below. The  $T_{CPE}$  parameter - as a measure of capacitive property - varied as follows: ILCP ( $T_{CPE} = 0.10 \text{ s}^{0.66} \Omega^{-1}$ )  $\gg$  ILPCP  $>$  Pt  $>$  GC  $\gg$  PCP ( $T_{CPE} = 4 \times 10^{-6} \text{ s}^{0.95} \Omega^{-1}$ ), paralleling the trend observed for background CV currents, with the ILCP exhibiting over three orders of magnitude higher  $T_{CPE}$  than the PCP. However, the latter, on account of its  $P_{CPE} = 0.95$ , was much more polarizable than the former ( $P_{CPE} = 0.475$ ). The two phase angle maxima observed for the ILPCP - interpreted as two time-constants (CPE-1 and CPE-2) - indicated the existence of two different conductive phases at the surface of this paste. CPE-1 was assigned to a PCP-like phase and CPE-2 to the ILCP-like phase.

### 3.3 Electrochemical Surface Probing with a Redox Probe

#### 3.3.1 Cyclic voltammetric electrode kinetics of the $[\text{Fe}(\text{CN})_6]^{3-/4-}$ redox system

Typical CVs at a scan rate ( $\nu$ ) of 100 mV/s in  $[\text{Fe}(\text{CN})_6]^{3-}$  (4 mM)/aq. KCl (0.1 M) are shown in Figure 5, with and without  $iR$ -drop and background current density ( $I_{bg}$ ) corrections. A pair of anodic and cathodic peaks for the redox probe was observed regardless of the electrode type.

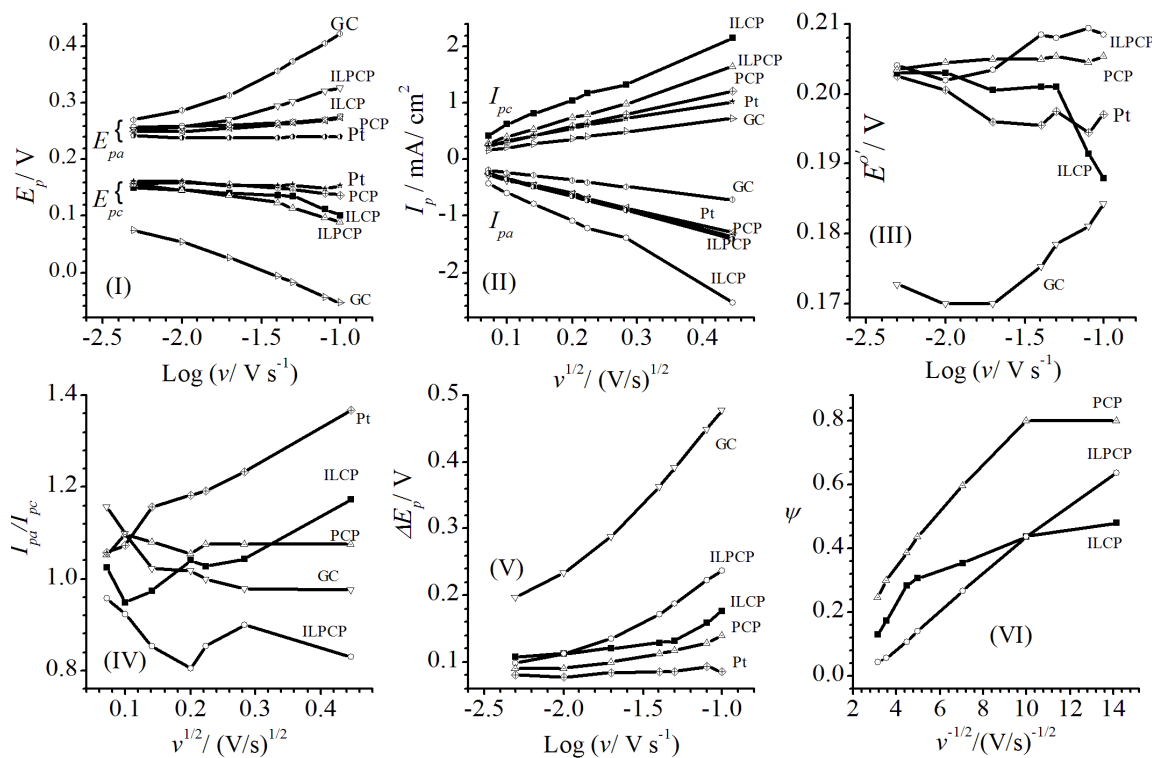


**Figure 6.** Dependence of CV parameters ( $E_{pa}$ ,  $E_{pc}$ ,  $E^{o'}$ ,  $\Delta E_p$ ,  $I_{pa}$ ,  $I_{pc}$ ,  $I_{pa}/I_{pc}$  ratio, and  $\psi$ ) for the  $[\text{Fe}(\text{CN})_6]^{3-/4-}$  (4 mM) redox probe as a function of scan rate ( $\nu$ ) in aq. KCl (0.1 M).

However, because of a high  $I_{bg}$  and consequently significant  $iR$ -drop error, peak potentials ( $E_p$ ) in the case of the ILPCP and ILCP electrodes were distorted (see Figures 5(IV) and (V)). Even though the PCP exhibited the highest  $R_{u-t}$ , its  $I_{bg}$  was not too high to cause significant  $iR$ -drop error. However, in the case of the ILPCP and ILCP, errors of about 0.030 V and 0.065 V were respectively evident. Therefore,  $iR$ -drop corrections were done on subsequently measured CVs before further data analysis. The  $R_{u-t}$  values determined with EIS were used for this purpose. Figure 5(VI) is an overlay of typical CVs for each of the electrodes after such corrections.

Various plots based on CVs of  $[\text{Fe}(\text{CN})_6]^{3-/4-}$  between 0.005 and 0.100 V/s scan rates have been shown in Figure 6(I) - (VI). According to the variation of peak separations ( $\Delta E_p$ ) with  $\log(v/\text{V s}^{-1})$ , this heterogeneous, one-electron transfer reaction ( $n = 1$ ) was found to be totally reversible (Er) on Pt surface ( $\Delta E_p \approx 0.084 \pm 0.005$  V constant), but largely quasi-reversible (Eqr) at lower scan rates or irreversible (Eir) at higher scan rate when it came to the GC ( $0.200 \text{ V} < \Delta E_p < 0.420 \text{ V}$ ). In the order of increasing dependence of  $\Delta E_p$  on  $\log v$ , or qualitatively according decreasing reaction speed: Pt (Er) > PCP (Er)  $\approx$  ILCP (Er) > ILPCP (Eqr)  $\gg$  GC (Eqr/ir).

**Table 2.** Electrochemical parameters evaluated for the  $[\text{Fe}(\text{CN})_6]^{3-/4-}$  redox system from Figure 6. (\*After dividing by  $\alpha^{1/2} = 0.707$  to partially offset the effect of irreversibility)

Parameter→	$A_{eff}/A_{geom}$	$A_{eff}/\text{cm}^{-2}$	$E^{\circ}/\text{V}$	$I_{pa}/I_{pc}$	$k^{\circ}/10^{-3}\text{ cm/s}$
Electrode↓/ Method →	$I_{pc}$ vs $v^{1/2}$	$I_{pc}$ vs $v^{1/2}$	Mean	Mean	$\psi$ vs $v^{1/2}$
Pt	0.94	0.0189	0.198±0.003	1.18±0.1	n/a
GC	0.88*	0.0622*	0.176±0.006	1.04±0.07	0.326
PCP	1.01	0.0204	0.205±0.001	1.07±0.02	2.88
ILPCP	1.32	0.0264	0.206±0.003	0.87±0.05	1.58
ILCP	1.83	0.0575	0.198±0.006	1.03±0.07	2.99

Table 2 lists standard heterogeneous rate constants ( $k^{\circ}$ ), effective electrochemical areas ( $A_{eff}$ ), mean formal potentials ( $E^{\circ} \approx (E_{pa} + E_{pc})/2$ ), and mean peak current ratios ( $I_{pa}/I_{pc}$ ), as well as  $A_{eff}/A_{geom}$  ratios as measures of electrode surface roughness. The ( $k^{\circ}$ ) were estimated with the method of Nicholson [66] for quasi-reversible systems based on Equation-3 as extended by Magno and co-workers [67] to Equation-4,  $\psi$  - being the Nicholson's dimensionless parameter,  $D_R$  and  $D_O$  respectively are the diffusion coefficient of  $[\text{Fe}(\text{CN})_6]^{4-}$  and  $[\text{Fe}(\text{CN})_6]^{3-}$ ,  $\alpha$  - the cathodic transfer coefficient, and the other symbols have their usual significances.  $D_R$  and  $D_O$  values of  $6.1 \times 10^{-5}$  and  $5.8 \times 10^{-5} \text{ cm}^2/\text{s}$  from the literature [68, 69], and  $\alpha$  was set as 0.5 according to several studies [70].

$$\psi = \left( \frac{RT}{FD_O\pi} \right)^{1/2} \left( \frac{D_O}{D_R} \right)^{\alpha/2} k^{\circ} v^{-1/2} \quad (\text{Equation-3})$$

$$\psi = \frac{-0.6288 + 0.0021 \times \Delta E_p}{1 - 0.017 \times \Delta E_p} \quad \text{(Equation-4)}$$

$$I_{pc} = 0.4463F \left( \frac{A_{eff}}{A_{geom}} \right) \left[ \frac{F}{RT} \right]^{1/2} C_O^{bulk} D_O^{1/2} \nu^{1/2} \quad \text{(Equation-5)}$$

The  $A_{eff}/A_{geom}$  and  $A_{eff}$  values were estimated from the slopes of the plots of cathodic peak current density ( $I_{pc}$ ) vs square root of scan rates ( $\nu^{1/2}$ ) using the Randles-Sevcik relation [60] for a reversible electrode reaction (Equation-5), where  $C_O^{bulk}$  stands for the bulk concentration of  $[\text{Fe}(\text{CN})_6]^{3-}$ . Accordingly, the ILCP was found to be of the highest roughness ( $A_{eff}/A_{geom} = 1.83$ ), followed by ILPCP ( $A_{eff}/A_{geom} = 1.32$ ) in general agreement with the conclusion reached above based on comparison of the constant phase element  $P_{CPE}$  parameters. Since for the rest of the electrodes the  $A_{eff}/A_{geom}$  ratios were almost unity, one may infer that the inclusion of the IL increased the  $A_{eff}$ . This may be understood as being the consequence of the increased number of electrocatalytic reaction sites brought about by the exfoliation of the graphite particles in the presence of the IL as suggested in based on SEM images in section 3.1 above and the literature [44, 46]. It has been known these reaction sites are predominantly found on the edges or edge planes and to some extent at defects in basal planes of the particles in question [71]. Furthermore, a recent molecular dynamics simulation study indicated that an IL monolayer would prefer to populate mainly the central surface rather than the edge planes of a graphene/ graphite particle, while paraffin mono-layers would be non-preferentially [72]. Thus, in an as made CP bulk or surface, the number of accessible electrocatalytic electron transfer sites would increase in the order  $\text{PCP} < \text{ILPCP} < \text{ILCP}$ , in accordance with the observed increase in the  $A_{eff}/A_{geom}$  ratio in the same order. Additional factors could be that the IL's molecules would more easily be stripped off the surface of the paste than paraffin molecules would be, thus creating more graphite/ graphene particles in direct contact with the electrolyte. Stripping of the binder liquid's molecules from the surface of a CP electrode could be brought about by either of or a combination of electrochemical, solvation [73] and electrophoretic processes, the last one being possible only in the case for the IL.

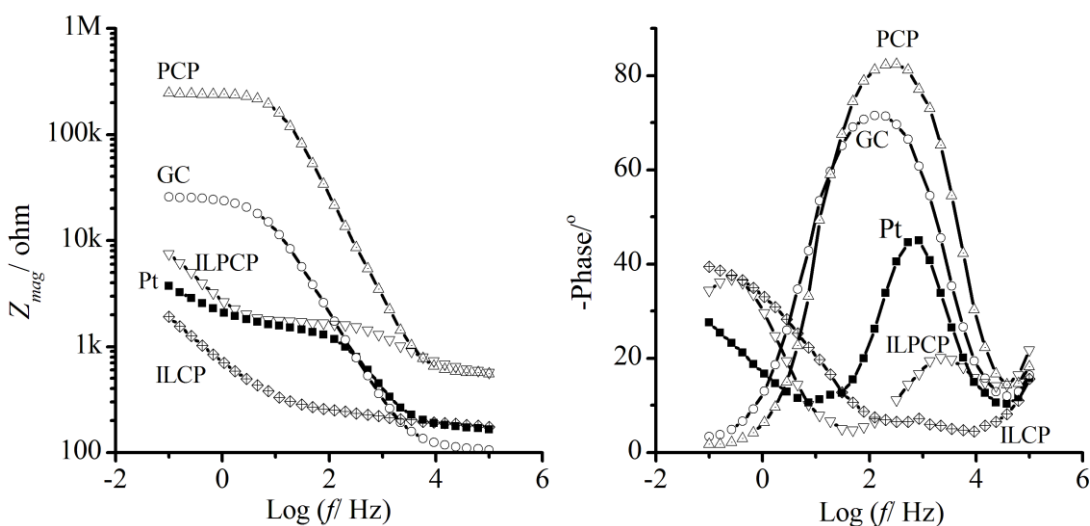


**Figure 7.** Bode plots for the CP, Pt and GC electrodes in aq. KCl (0.1 M) in the presence of  $[\text{Fe}(\text{CN})_6]^{3-/4-}$  (8 mM; 1:1).  $E_{ac} = 10$  mV, bias  $E_{dc} = 0.170$  V for ILCP, else 0.200 V

According to Figure 6(II) the highest  $I_p$  was observed with the ILCP and the lowest one with the GC. In decreasing order:  $I_p(\text{ILCP}) > I_p(\text{ILPCP}) > I_p(\text{PCP}) \approx I_p(\text{Pt}) > I_p(\text{GC})$ , almost mirroring the trend in  $A_{\text{eff}}/A_{\text{geom}}$  ratios as well as the  $A_{\text{eff}}$  values (except for the GC electrode). Despite the GC electrode having the largest  $A_{\text{eff}}$  and  $A_{\text{eff}}/A_{\text{geom}}$  ratio comparable to Pt and PCP, the fact that  $I_p(\text{GC})$  was the lowest could be ascribed to the electrode reaction at this electrode being the most kinetically controlled as the corresponding  $\Delta E_p$  or  $k^0$  were the largest or the smallest among the five electrodes compared. No significant differences in  $k^0$  was observed between the three CP electrodes (Table 2). Thus, the increase in  $A_{\text{eff}}$  or the number of accessible electron transfer sites might have only resulted in the enhancement of the rate of electron transfer without affecting the rate constant and similar electrocatalytic reaction sites were involved. Plots of peak current density ratios ( $I_{pa}/I_{pc}$ ) and their statistical mean values are also presented in Figure 6(IV) and Table 2, respectively. The ratios found for the different electrodes were practically closely clustered around unity, except the deviations observed in case of the Pt electrode which suffered interference from a background peak (see Figure 2 (Pt)) resulting in an apparent increase in this ratio with the scan rate.

Formal redox potentials ( $E^{\circ}$ ) of  $[\text{Fe}(\text{CN})_6]^{3-}$  have been plotted against  $\log(v/V\text{ s}^{-1})$  in Figure 6(III). Statistical mean values of  $E^{\circ}$  over the studied scan rates are also listed in Table 2. The  $E^{\circ}$  at each electrode was generally clustered around the respective mean value. In the case of the Pt the apparent cathodic shift in  $E^{\circ}$  was caused by errors introduced by an interfering background peak already mentioned. Except for GC, similar  $E^{\circ}$  values were observed regardless of the electrode type: ILPCP (0.206 V), ILCP (0.198 V), Pt (0.198 V) = PCP (0.205 V), and GC (0.176 V) indicating the thermodynamic equivalence of these surfaces with respect to  $[\text{Fe}(\text{CN})_6]^{3-/4-}$  electrochemistry.

### 3.2.2 Impedance spectroscopic electrode kinetics of the $[\text{Fe}(\text{CN})_6]^{3-/4-}$ redox system

**Table 3.** Equivalent circuit characteristics based on the models in Figure 4 and parameters quantities extracted after CNLS fitting of the EIS results in Figure 7. Recalculated using  $A_{\text{eff}}$  instead of  $A_{\text{geom}}$

Electrode	$R_{ct}/$ k $\Omega$	$R_{ct} \times A_{\text{eff}}/$ k $\Omega$ cm <sup>2</sup>	$T_{CPE}/$ 10 <sup>-6</sup> s <sup>P</sup> $\Omega^{-1}$	$P_{CPE}$	$T_{CPE}/A_{\text{eff}}/$ 10 <sup>-6</sup> s <sup>P</sup> $\Omega^{-1}$ cm <sup>-2</sup>	$I_o/$ $\mu\text{A cm}^{-2}$	$k^o/$ 10 <sup>-3</sup> cm/s
Pt	1.36	0.0257	1.47	0.874	77.8	998	2.58
GC	25.4	1.58	1.71	0.872	27.5	16.2	0.0421
PCP	241	4.92	0.068	0.976	3.3	5.23	0.0136
ILPCP	0.991	0.0262	0.7	0.795	26.5	74.8	0.194
	13	0.343	156	0.75	5909.1	981	2.54
ILCP	0.026	0.0015	2.5	1.000	43.5	17176	44.5
		-	719	0.505	12504.3	-	-

Impedance spectra (Bode plots) recorded in the presence of  $[\text{Fe}(\text{CN})_6]^{4-}$  (4 mM) and  $[\text{Fe}(\text{CN})_6]^{3-}$  (4 mM) are shown in Figure 7. Table 3 presents the values of the equivalent circuit elements or parameters as obtained by CNLS fitting of these data to the respective models in Figure 4.

$R_{u-t}$  and  $CPE$  parameters of similar order of magnitude as those determined in the absence of  $[\text{Fe}(\text{CN})_6]^{3-/4-}$  in aq. KCl were found for all the electrodes. But, the  $R_{ct}$ , hence, the  $I_o$ , was significantly different from the corresponding background ( $I_{o,bg}$ ) values (Table 1). For the Pt and GC electrodes, the respective  $I_{o,bg}$  contributed only about 1% to the total  $I_o$  in the presence of  $[\text{Fe}(\text{CN})_6]^{3-/4-}$  (8 mM), 1:1), while for PCP and ILPCP this was 10% and 13%, respectively. Furthermore the equivalent circuit for the ILPCP electrode still contained two time-constants, whereas that for the ILCP now incorporated a new resistor/capacitor (RC) element in series with the CPE element.

$k^o$  values for the electrode reaction in question were calculated according to Equation-6 [60] from the respective  $I_o$  without the need for background correction, but using  $A_{eff}$  instead of  $A_{geom}$ . Unlike the magnitudes estimated in the previous section using the CV data, the  $k^o$  values here varied significantly across the different types of electrodes. The ILCP electrode exhibited the highest ( $4.5 \times 10^{-2}$  cm/s), and PCP the lowest ( $1.4 \times 10^{-5}$  cm/s)  $k^o$  according to the trend:  $k^o$  (ILCP)  $\gg$   $k^o$  (Pt)  $\approx$   $k^o$  (ILPCP)  $\gg$   $k^o$  (GC)  $>$   $k^o$  (PCP). There was also no consistency both in magnitude and trend between the  $k^o$  estimated by EIS and those by CV. This might be because of the greater sensitivity of the EIS technique in connection with its requirement of a strictly long-term steady state for accurate measurement data to be obtained; therefore the  $k^o$  found from CV should be more reliable.

$$k^o = \frac{I_o}{F(C_R^{bulk})^\alpha (C_O^{bulk})^{1-\alpha}} \quad (\text{Equation-6})$$

#### 4. CONCLUSIONS AND PROSPECTS

The IL, 1-methyl-3-octylimidazolium bis(trifluoromethyl-sulfonyl)imide, was successfully applied as the binding liquid for the first time to prepare CP electrode materials ILCP and ILPCP despite exhibiting increased  $I_{bg}$  unlike the PCP. A large proportion of the graphite particles in the pastes were coated with the liquid binder, but the IL bound the particles more efficiently resulting in more compact pastes than paraffin did. In the former case the particles appeared to have been transformed into thinner sheets (flakes). Nevertheless, its attractive features include wide electrochemical windows of ILCP (+2.5 V) and ILPCP (+2.2 V) and smooth background CVs similar with the PCP's but superior to Pt and GC electrodes in aq. KCl. Unlike PCP, ILCP, Pt, and GC electrodes, the ILPCP had two distinct conductive phases. Its ohmic resistivity was found to be much smaller than PCP and ILPCP. Formal potentials obtained for the  $[\text{Fe}(\text{CN})_6]^{3-/4-}$  redox system using CVs were similar among the CPs ( $E^o \approx 0.200$  V). While the  $A_{eff}/A_{geom}$  increased according to PCP  $<$  ILPCP  $<$  ILCP, the  $k^o$  determined by this method did not vary significantly with the paste composition, thus, the incorporation of the IL only increased the effective electrochemical area. In the future, the ILCP and ILPCP electrodes will be tested as direct amperometric sensors and as platform for developing modified electrodes to be used in supercapacitors, batteries, and biosensors. An intermediate application of the ILPCP paste in the electrodeposition of films of Fe and Mn oxides and hydroxides will be reported soon.

## ACKNOWLEDGEMENT

We gratefully acknowledge financial supports from the National Research Foundation (NRF, South Africa) and Department of Science and Technology (DST, South Africa); and CSIR (Pretoria) for letting us use the JEOL- JSM 7500F field emission electron microscope.

## References

1. J.-f. Liu, G.-b. Jiang, J.-F. Liu, and J.Å. Jönsson, *TrAC Trends in Anal. Chem.*, 24 (2005) 20
2. S.F. Wang, H.Y. Xiong, and Q.X. Zeng, *Electrochem. Commun.*, 9 (2007) 807
3. I. Svancara and K. Schachl, *Chemické Listy*, 93 (1999) 490
4. I. Svancara, K. Vytras, J. Barek, and J. Zima, *Crit. Rev. in Anal. Chem.*, 31 (2001) 311
5. M. Opallo and A. Lesniewski, *J. Electroanal. Chem.*, 656 (2011) 2
6. H. Liu, P. He, Z. Li, C. Sun, L. Shi, Y. Liu, G. Zhu, and J. Li, *Electrochem. Commun.*, 7 (2005) 1357
7. Y. Liu, X. Zou, and S. Dong, *Electrochem. Commun.*, 8 (2006) 1429
8. A. Safavi, N. Maleki, O. Moradlou, and F. Tajabadi, *Anal. Biochem.*, 359 (2006) 224
9. R.T. Kachoosangi, G.G. Wildgoose, and R.G. Compton, *Electroanal.*, 19 (2007) 1483
10. L. Zheng, J.-q. Zhang, and J.-F. Song, *Electrochim. Acta*, 54 (2009) 4559
11. C. Díaz, C. García, P. Iturriaga-Vásquez, M.J. Aguirre, J.P. Muena, R. Contreras, R. Ormazábal-Toledo, and M. Isaacs, *Electrochim. Acta*, 111 (2013) 846
12. H. Gao, X. Qi, Y. Chen, and W. Sun, *Anal. Chim. Acta*, 704 (2011) 133
13. T. Zhan, L. Cao, W. Sun, and W. Hou, *Anal. Methods*, 3 (2011) 2651
14. M. Arvand, A. Niazi, R.M. Mazhabi, and P. Biparva, *J. Mol. Liq.*, 173 (2012) 1
15. A.A. Ensafi, H. Bahrami, B. Rezaei, and H. Karimi-Maleh, *Materials Sci. and Eng.: C*, 33 (2013) 831
16. Y.-M. Zhang, C.-Q. Duan, and Z.-N. Gao, *J. Serb. Chem. Soc.*, 78 (2013) 281
17. B. Haghighi, L. Nazari, and S.M. Sajjadi, *Electroanal.*, 24 (2012) 2165.
18. L. Lu, X. Huang, and Y. Qu, *J. Solid State Electrochem.*, 16 (2012) 3299
19. W. Sun, X. Wang, X. Sun, Y. Deng, J. Liu, B. Lei, and Z. Sun, *Biosens. Bioelectron.*, 44 (2013) 146
20. N.F. Atta, A. Galal, S.M. Azab, A.H. Ibrahim, *J. Electrochem. Soc.*, 162 (2015) B9-B15
21. F. Faridbod, M.R. Ganjali, B. Larijani, and P. Norouzi, *Electrochim. Acta*, 55 (2009) 234
22. H. Dai, H. Xu, X. Wu, Y. Chi, and G. Chen, *Anal. Chim. Acta*, 647 (2009) 60
23. M. Pandurangachar, B.E. Kumara Swamy, B.N. Chandrashekar, O. Gilbert, and B.S. Sherigara, *J. Mol. Liquids*, 158 (2011) 13
24. S. Hu, Y. Wang, X. Wang, L. Xu, J. Xiang, and W. Sun, *Sens. Actuators, B*, 168 (2012) 27
25. R. Mirshafian, M.R. Ganjali, and P. Norouzi, *Int. J. Electrochem. Sci.*, 7 (2012) 1656
26. X. Yu, Y. Chen, L. Chang, L. Zhou, F. Tang, and X. Wu, *Sensors and Actuators B: Chemical*, 186 (2013) 648
27. T. Tavana, M.A. Khalilzadeh, H. Karimi-Maleh, A.A. Ensafi, H. Beitollahi, and D. Zareyee, *J. Mol. Liquids*, 168 (2012) 69
28. J. Vahedi, H. Karimi-Maleh, M. Baghayeri, A.L. Sanati, M.A. Khalilzadeh, and M. Bahrami, *Ionics*, 19 (2013) 1907
29. Y. Zhang, F.-y. Du, and J.-j. Xue, *Lihua Jiannan, Huaxue Fence*, 47 (2011) 1100.
30. R. Ojani, J.-B. Raoof, and S. Zamani, *Applied Surface Science*, 271 (2013) 98.
31. P. Macikova, V. Halouzka, J. Hrbac, P. Bartak, and J. Skopalova, *The Scientific World Journal*, 2012 (2012) 1
32. C.-L. Yu, N.-C. Lo, H. Cheng, T. Tsuda, T. Sakamoto, Y.-H. Chen, S. Kuwabata, P.-Y. Chen, *J. Electroanal. Chem.*, 729 (2014) 109-115
33. Q.-j. Niu, J. Liu, G.-j. Li, H.-q. Qin, H.-w. Gao, and W. Sun, *J. Chin. Chem. Soc. (Weinheim, Ger.)*,

667 (2012) 667

34. F. Shi, H. Zhu, L. Li, L. Ling, and W. Sun, *J. Chin. Chem. Soc.*, 60 (2013) 1285
35. M. Noroozifar, M. Khorasani-Motlagh, M.B. Parizi, and R. Akbari, *Ionics*, 19 (2013) 1317
36. H. Gao, M. Xi, X. Qi, M. Lu, T. Zhan, and W. Sun, *J. Electroanal. Chem.*, 664 (2012) 88
37. X. Zhai, L. Li, H. Gao, C. Si, and C. Yue, *Microchim. Acta*, 177 (2012) 373
38. H. Gao, Y. Duan, L. Xu, and W. Sun, *Croat. Chem. Acta*, 84 (2011) 33
39. L. Liu, Y. Cheng, F. Sun, J. Yang, and Y. Wu, *J. Solid State Electrochem.*, 16 (2012) 1003
40. C. Ruan, Z. Sun, S. Lu, L. Li, J. Lou, W. Sun, *Russ. J. Electrochem.*, 50 (2014) 129-135
41. A.L. Sanati, H. Karimi-Maleh, A. Badiiei, P. Biparva, A.A. Ensafi, *Mater. Sci. Eng., C* 35 (2014) 379-385
42. H. Tokuda, S. Tsuzuki, M.A.B.H. Susan, K. Hayamizu, and M. Watanabe, *J. Phys. Chem. B*, 110 (2006) 19595
43. T.T. Waryo, S. Begic, E. Turkusic, K. Vytras, and K. Kalcher in *Sensing in Electroanalysis* K. Vytras and K. Kalcher (Editor(s)), University of Pardubice, Pardubice (2005) p. 145-191.
44. X. Zhang, M. Li, J. Zhao, B. Chena, K. Qua, *J. Chin. Chem. Soc.*, 60 (2013) 437-439
45. Y. Li, X. Zhai, X. Liu, L. Wang, H. Liu, H. Wang, *Talanta*, 148 (2016) 362–369
46. X. Zhang, M. Li, Y. Cui, J. Zhu, J. Zhao, B. Chen, K. Qu, *Int. J. Electrochem. Sci.*, 8 (2013) 4839 – 4849
47. H. Gunzler, H.U. Gremlich, *IR Spectroscopy - An Introduction*, WILEY-VCH, Weinheim (2002)
48. J.W. Robinson, E. M. S. Frame, G. M. Frame, *Undergraduate instrumental analysis*, 6<sup>th</sup> Ed., Marcel Dekker, New York (2005)
49. D.R. Lide (Edr), *CRC Handbook of chemistry and physics*, CRC Press (2002)
50. M. Pandurangachar, B.E. Kumara Swamy, B.N.Chandrashekar, Ongera Gilbert, Sathish Reddy, B. S.Sherigara, *Int. J. Electrochem. Sci.*, 5 (2010) 1187 – 1202
51. G. Shul, J. Sirieix-Plenetm, L. Gaillon, M. Opallo, *Electrochemistry Communications* 8 (2006) 1111–1114
52. A. Wang, D.D. L, Chung, *Carbon* 72 (2014) 135-151
53. M. Muti, A. Erdema, A. Caliskana, A. Sinagc, T. Yumak, *Colloids and Surfaces B: Biointerfaces* 86 (2011) 154–157
54. W. Sun, L. Xu, J. Liu, X. Wang, S. Hu, and J. Xiang, *Croat. Chem. Acta* 86 (2013) 129–135
55. H. N. A. Mustafa, I. M. Isa, N. M. Ali, N. Hashim, M. Musa, S. A. Ghani, *Int. J. Electrochem. Sci.*, 10 (2015) 9232 - 9245
56. G. Hsieh, T.O. Mason, and L.R. Pederson. *Solid State Ionics*, 91 (1996) 203
57. A. Lasia, *Electrochemical Impedance Spectroscopy and its Applications*, in *Modern aspects of electrochemistry*, B.E. Conway, Bockris, J., and White, R.E. (Editor(s)), Kluwer Academic/ Plenum Publishers: New York (1999) p.143-248
58. Z.B. Stoynov, B.M. Grafov, B. Savova-Stoynova, and V.V. Elkin, *Elektrokhimicheskii impedans (The Electrochemical Impedance)*, Nauka, Moscow (1991)
59. M.G. Astaf'ev, *Russ. J. Electrochem.*, 36 (2000) 274
60. A.J. Bard and L.R. Faulkner, *Electrochemical methods, Fundamental and applications*, John Wiley & Sons, New York (2000)
61. D.R. Lide, *Handbook of chemistry and physics*, CRC PRESS (2000)
62. M. Strojnik, *Proc. SPIE-Int. Soc. Opt. Eng.*, 6307 (2006) 63070S/1
63. R.L. Powell and G.E. Childs, *American Institute of Physics handbook*, B.H. Billings and D.E. Gray (Editor(s)), McGraw-Hill, New York (1972)
64. A. Cezairliyan and A.P. Müller, *Int. J. Thermophys.*, 6 (1985) 285
65. [www.engineeringtoolbox.com/](http://www.engineeringtoolbox.com/). *Reistivity-conductivity-d\_418*. 2011; Available from: [Http://www.engineeringtoolbox.com/resistivity-conductivity-d\\_418.html](http://www.engineeringtoolbox.com/resistivity-conductivity-d_418.html).
66. R.S. Nicholson, *Anal. Chem.*, 37 (1965) 1351
67. I. Lavagnini, R. Antiochia, and F. Magno, *Electroanalysis*, 16 (2004) 505

68. T.J. Davies, R.R. Moore, C.E. Banks, and R.G. Compton, *J. Electroanal. Chem.*, 574 (2004) 123
69. T.J. Davies, S. Ward-Jones, C.E. Banks, J. del Campo, R. Mas, F.X. Muñoz, R.G. Compton, *J. Electroanal. Chem.*, 585 (2005) 51
70. D.H. Angell and T. Dickinson, *J. Electroanal. Chem. and Interf. Electrochem.* 35 (1972) 55
71. M. Pumera, *Chem. Soc. Rev.*, 39 (2010) 4146-4157
72. M. H. Ghatee, S. Namvar, A. R. Zolghadr, F. Moosavi, *Phys. Chem. Chem. Phys.*, 17 (2015) 24722-24731
73. I. Svancara, K. Vytras, J. Barek, and J. Zima, *Crit. Rev. in Anal. Chem.*, 31 (2001) 311

© 2016 The Authors. Published by ESG ([www.electrochemsci.org](http://www.electrochemsci.org)). This article is an open access article distributed under the terms and conditions of the Creative Commons Attribution license (<http://creativecommons.org/licenses/by/4.0/>).